Composites Part A 117 (2019) 357–368

Contents lists available at ScienceDirect

Composites Part A

journal homepage: www.elsevier.com/locate/compositesa

Mechanical properties and impact performance of silk-epoxy resin composites modulated by flax fibres

Change Wu[a,b,1], Kang Yang[a,1], Yizhuo Gu[a], Jun Xu[c], Robert O. Ritchie[d,*], Juan Guan[a,b,*]

[a] Intl. Research Center for Advanced Structural and Biomaterials, School of Materials Science and Engineering, Beihang University, Beijing 100191, China
[b] Beijing Advanced Innovation Center for Biomedical Engineering, Beihang University, Beijing 100083, China
[c] Department of Automotive Engineering, School of Transportation Science and Engineering and Advanced Vehicle Research Center (AVRC), Beihang University, Beijing 100191, China
[d] Materials Sciences Division, Lawrence Berkeley National Laboratory and Department of Materials Science & Engineering, University of California, Berkeley CA94720, USA

ARTICLE INFO

Keywords:
Natural fibers
Impact behaviour
Resin transfer moulding (RTM)

ABSTRACT

Silk fibres possess good biodegradability, excellent biocompatibility and moderate modulus and stiffness, whereas flax fibres are low cost, renewable natural fibres with high specific strength and modulus. Here we introduce economical flax fibres to modulate the stiffness and impact properties of natural *B. mori* silk reinforced epoxy composites fabricated via vacuum-assisted resin transfer moulding. Intra-and inter-hybridizations of flax and silk fibres are applied to evaluate the effect on composite mechanical properties including tensile and flexural modulus and strength. The interface properties between the fibres and matrix are investigated using dynamic mechanical thermal analysis (DMTA). Most importantly, falling weight impact experiments reveal that silks can effectively prevent crack propagation whereas flax fibres can greatly enhance the impact load. Our study could offer new solutions towards novel biocomposites with tailored modulus, strength and toughness properties based on natural biopolymer fibres.

1. Introduction

In recent years, natural fibres have been increasingly used as reinforcements for applications in the automotive industry and for sports equipment [1,2]. Natural fibres from plants or animals are more environmentally friendly and could be less costly than synthetic fibres [3]. Despite their known merits such as low cost, light-weight, biodegradability and good mechanical properties, common natural fibres may be restricted for wider applications in structural composites due to their large variability, poor toughness and low impact resistance [4]. Flax fibres, however, have been one most popular plant fibres as a “green” and low-cost reinforcement [5]. They have superior mechanical properties to most plant fibres and specific mechanical properties comparable to glass fibres [6–9], which makes them a competitor to glass fibres for various composite applications. However, the low interlaminar strength and poor fracture toughness of flax fibres due to their weak interfacial bonding have restricted their industrial use [10]. Coating methodologies (*e.g.*, incorporate modified carbon nanotubes (CNTs) [6]) and hybridization with glass fibres [11] have been applied to improve the interfacial strength and fracture toughness of flax reinforced composites. Nevertheless, the incorporation of nanomaterials would markedly increase the cost of raw materials and processing, which is not advantageous.

Natural silks such as silks from silkworms as a single or hybrid fibre reinforcement have been utilized to improve flexural and impact mechanical properties of epoxy resin composites [12]. Silk fibres can absorb and dissipate energy simultaneously during deformation, which results in excellent mechanical toughness [13–15]. Notably, silk reinforced epoxy resin composites exhibit much higher tensile and flexural strains at break compared to plant fibre and glass fibre reinforced composites (PFRP/GFRPs) [16]. In addition, they can be made with high reinforcement volume fractions; in fact, as high as 70 vol% silk reinforcement has been achieved in epoxy composites using compression moulding [17]. In the same work, the impact strength of 60 vol% silk epoxy resin composites was found to be six times higher than that for the pure epoxy resin. Moreover, silk reinforcement can improve the

* Corresponding authors at: School of Materials Science and Engineering, Beihang University, Beijing 100191, China (J. Guan). Lawrence Berkeley National Laboratory and Department of Materials Science & Engineering, University of California, Berkeley, CA 94720, USA (R.O. Ritchie).

E-mail addresses: roritchie@lbl.gov (R.O. Ritchie), juan.guan@buaa.edu.cn (J. Guan).

[1] Equal contribution first author.

https://doi.org/10.1016/j.compositesa.2018.12.003
Received 16 August 2018; Received in revised form 15 November 2018; Accepted 6 December 2018
Available online 07 December 2018
1359-835X/

ductility and overall breaking energy of the epoxy composites at sub-ambient temperatures, as low as −50 °C [18]. It has also been suggested that silk fibres have the potential to be exploited in energy-absorbing applications [4,6,7,19–21]. Nevertheless, the moderate strength and modulus of natural silks may offset their relatively high ductility and toughness. Specifically, natural silk fibres from silkworms have a 5–15 GPa tensile modulus, 300–600 MPa tensile strengths with 15–25% failure strains [4,16,20]. Additionally, the interfacial bonding between the silk and epoxy resin has been found to exceed that between plant fibres and epoxy resin [17].

Hybridization of reinforcement fibres with complementary characteristics is a popular strategy to balance the cost, mechanical properties and "green" credentials of the composite. For example, the combination of carbon/glass fibres [22] with the carbon fibres as top and bottom layers can effectively increase damage tolerance under impact. Hybridization of synthetic fibres with natural fibres, and of natural fibres with other natural fibres, has also attracted increasing attention of late [21,23–26]. An example of this is hybridizing basalt (from natural stones) with carbon fibres to improve impact performance [23]; basalt fibres have also been chosen as hybridization fibres to improve the impact performance of flax fibre reinforced composites [10,14,15]. Natural silk fibres have also been hybridized with other fibres [27–29]. In particular, the improved fatigue resistance of silk has been used in hybridized composites as silk fibres appear to possess the capacity of slowing down the crack propagation process [30]. Additionally, the mechanical strength of hybrid composites has been enhanced by adding short silk fibres into glass fibre reinforced epoxy composites, where it has been claimed that the short silk fibre may facilitate stress transfer under tensile loading by acting as bridges [31]. In addition to advantages in mechanical properties, silk fibre hybridization also can have beneficial effects on the physical properties of composites, such as light transmission and luminance distribution ability [32].

To our knowledge, hybridization of the two biopolymer fibres, that of silk and flax fibres, has not been studied to improve the mechanical properties and impact performance of epoxy resin matrix composites. In this work, we question whether high-modulus flax fibres can modulate the modulus of silk reinforced epoxy resin composites, and whether the high ductility and toughness of silk fibres are compromised through hybridization. Accordingly, we introduced controlled flax fibre fractions into silk fibre reinforced epoxy resin composites, which were fabricated through a Vacuum-Assisted Resin Transfer Moulding process (VARTM). The effects of flax fibre content and hybrid configuration were studied on the mechanical properties and impact performance of silk fibre composites. The intent of this work is to provide new insights into designing "greener" bio-composites with enhanced mechanical properties.

2. Materials and methods

2.1. Materials

A plain woven *Bombyx mori (B. mori)* silk fabric with an areal density of 90 ± 5 g.m^{-2}, and three plain woven (*B. mori*) silk-flax hybrid fabrics (mixed ratios of flax/silk of 30/70, 21/79, and 42/58) with respective areal densities of 60 ± 5 g.m^{-2}, 80 ± 5 g.m^{-2} 120 ± 5 g.m^{-2}, were obtained from Hu Zhou Yong Rui Textile Co. Ltd (Zhejiang, China). A plain-woven flax fabric with an areal density of ~ 145 g.m^{-2} was purchased from Yi Bai Wang Industry Store. The densities of the silk and flax fibre were reported to be 1300 kg.m^{-3} and 1450 kg.m^{-3} respectively [16,33].

A low viscosity (for easy flow in VARTM) epoxy resin system labelled Araldite LY1564/Aradur3486 (epoxy resin/hardener) produced by the Huntsman Corporation (US) was acquired, with a specified density at room temperature of 1.1–1.2 × 10^3 kg.m^{-3}; its curing ratio was 100:34 by weight with curing conditions of 80 °C for 8 hrs. The chemical structures of the epoxy system 1564 including a bisphenol epoxy and an aliphatic epoxy and the chemical structure of the hardener system 3486 are shown in Appendix I.

2.2. Fabrication of hybrid composites

Hybrid composites were fabricated as laminates using a VARTM setup, as shown in Fig. 1(a), followed by hot pressing to obtain a high volume fraction of the fibre and improved interface quality of the composite [34,35]. All the fabrics were cut to dimensions of 200 mm × 100 mm and dried in a vacuum oven at 70 °C for 12 hrs prior to resin infusion (as natural fibres tend to have ~ 5% moisture content) [21]. The number of plies was calculated to keep the laminate volume fraction at roughly 50%. After drying, the reinforcement fabrics were laid on the mould, and a peel ply and distribution media were also added to the top and bottom. The entire assembly was covered with a vacuum bag and sealed with sealant. A low viscosity resin system was used to facilitate fibre wetting. Resin-hardener mixture was allowed to degas for 30 mins in a vacuum chamber, prior to impregnation through VRATM [7,24] After the entire layup was impregnated, the resin system was allowed to fully infiltrate for 15 mins. Then the layup was moulded and hot pressed at a pressure of 500 kPa for 8 hrs at 80 °C to complete the curing reaction.

Fig. 1(b,c) shows the fibre fractions and hybrid configurations of the silk and hybrid laminates developed for this study; all laminates had an overall fibre volume fraction of approximately 50 vol% and a thickness of 2 mm. The relative volumes of silk versus flax fibres were achieved through variations in hybrid fabrics and configurations. The silk laminates from *B. mori* reinforcement fibre were termed SB. For the intraply hybrid laminates, three variations of (*B. mori)* silk/flax hybrid fabrics have mix ratios of 42/58, 30/70, 21/79; the final composites are termed as FS1, FS2, FS3 accordingly with increasing flax content. For the super-hybrid laminates (including both intraply and interply), *B. mori* silk fabrics and 30/70 silk-flax hybrid fabrics were used in two super-hybrid configurations. For the first configuration, six silk fabrics as the core and five 30/70 silk-flax hybrid fabrics as skins were stacked as a sandwich, which is termed as HSH. Similarly, SHS applied silk fabrics as skins and hybrid fabrics as the core. For the second configuration, eight 30/70 silk-flax hybrid layers and seven silk fibre fabrics were alternatively plied, keeping silk-flax hybrid layers as the outermost layers; this is termed as SHI.

2.3. Microstructure and morphology analyses

The morphology and microstructure of the plain weave fabrics and fractured cross section of the fabricated laminates were imaged under an optical microscope (Shanghai Optical Instruments Co. Ltd., China) and a scanning electron microscope (SEM, JEOL JSM−6010, Japan). A 20 kV accelerating voltage and the secondary electron image mode were used to take all SEM images.

2.4. Quasi-static mechanical testing

Uniaxial tensile mechanical properties of the composites were measured in accordance with the Chinese Standard GB/T1040-92 using an Instron 8801 screw-driven testing machine (Instron Corp., Norwood, MA, USA), operating at a displacement rate of 2 mm.min^{-1} with an extensometer (Instron, Catalogue no. 2620-601) mounted on the sample to measure strain. The dimensions of the tested dog-bone specimens were 115 mm × 25 mm × 2 mm with a gauge length of 10 mm.

Flexural mechanical properties were evaluated with unnotched specimens tested in three-point bending on an Instron 5565 screw-driven testing machine, also at a cross-head speed of 2 mm.min^{-1}, in accordance with the Chinese Standard GB/ T1449-2005. The specimens were rectangular in cross-section with dimensions of 40 mm × 15 mm × 2 mm.

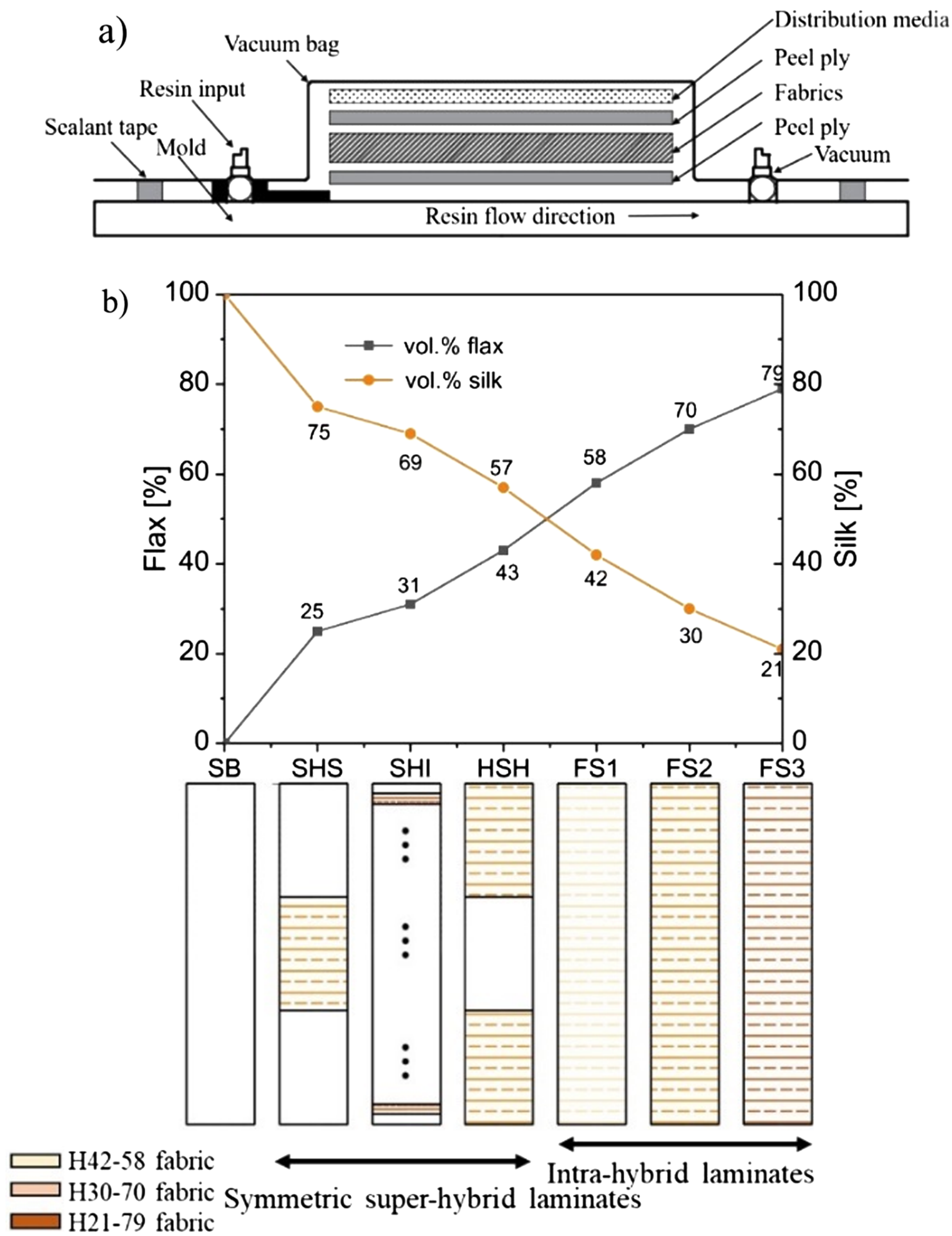

Fig. 1. (a) Illustration of VARTM set-up and fabrication, showing (b) the relative volume fractions of silk/flax fibres in the fibre reinforcements and configurations of hybrid composites.

The interlaminar shear strength was evaluated in accordance with the International Standard ISO 14130:1997 on the same Instron 5565 machine at a cross-head speed of 1 mm.min^{-1}. All the specimens were cut out from laminates by water-cutting method to a dimensional accuracy of ± 0.1 mm. The specimens were also rectangular in cross-section with dimensions of 20 mm × 10 mm × 2 mm.

2.5. Impact testing

Toughness properties of the composites were assessed using un-notched Charpy impact specimens on a pendulum impact testing machine (MTS model ZBC 1000, MTS Corp., Eden Prairie, MN, USA), in accordance with the International Standard ISO 179:1997. 4 J impact energy calculated from the impactor mass and initial height was used to load onto specimens.

The falling weight impact mechanical properties were evaluated in accordance with ASTM D7136 standard on an in-house built impact machine with a 1.723 kg impactor comprising a 12.7 mm diameter hemispherical nose [36]. The force applied to the impactor by the sample was recorded by the force sensor and stored by the digital phosphor oscilloscope (Tektronix; DPO 2014B) as a function of time. In our study, laminate specimens with dimensions of 100 mm × 100 mm × 2 mm were tightly clamped by two plates with a central 76-mm diameter circular opening of depth 18 mm on the upper plate (total mass of 9.55 kg) which was located straight under the impactor [37]. A 3 J impact energy was initially used in the experiments, but was increased to 4 J (by increasing the height of the impactor from 180 to 240 mm) as the lower impact energy did not penetrate some specimens.

2.6. Dynamic mechanical thermal analysis

The thermo-mechanical properties of the silk and hybrid fibre composites were also evaluated by dynamic mechanical thermal analysis (DMTA), measured using a DMA Q800 instrument (TA Instrument, Waters Ltd.) under cantilever mode with a heating rate of 3 °C min^{-1}, at

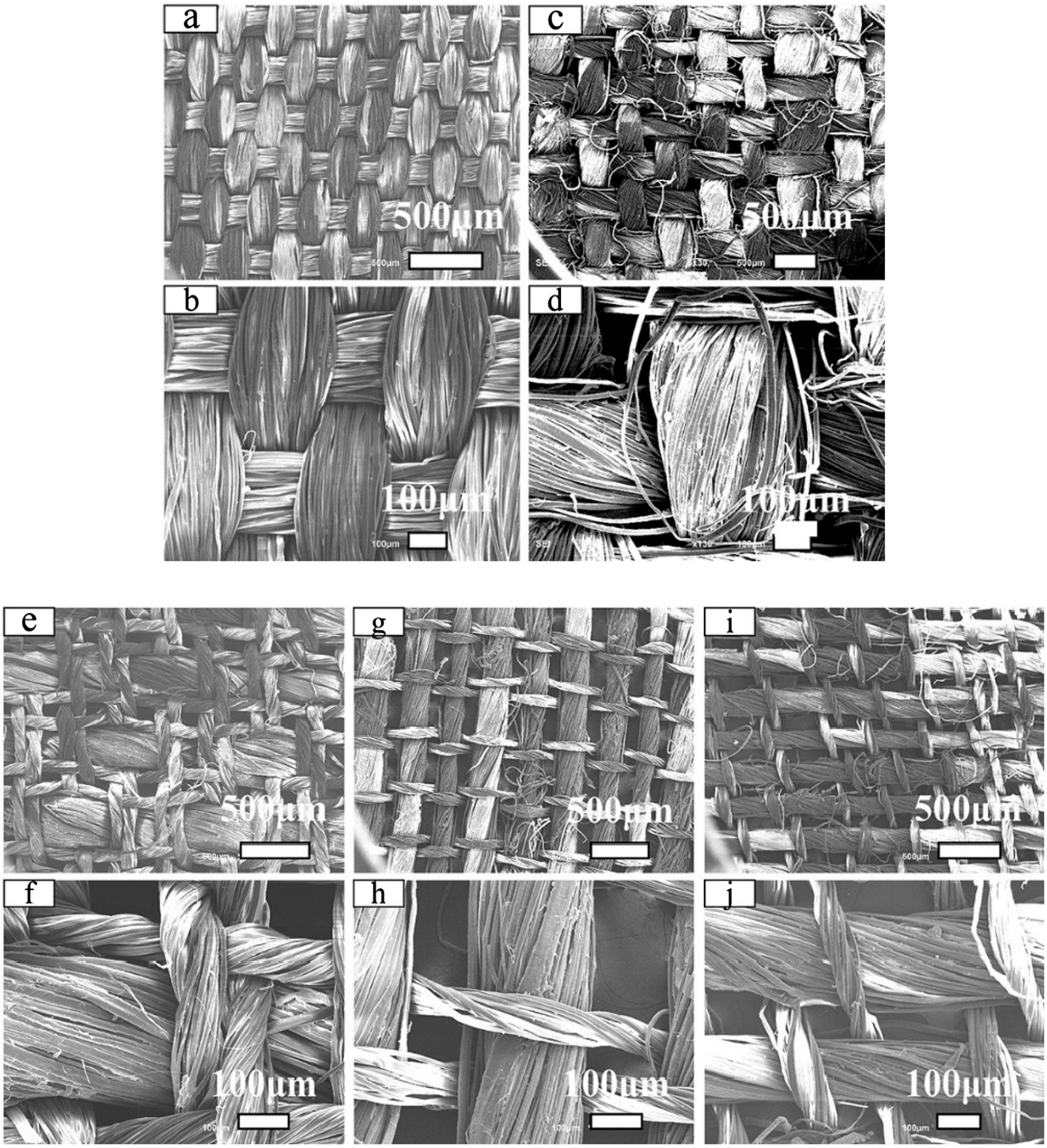

Fig. 2. Scanning electron microscope (SEM) images of the microstructure of the plain weave fabrics (a, b) *B.mori* silk, (c, d) flax, (e, f) hybrid H21-79, (g, h) H30-70, and (i, j) H42-58. The enlarged images in (b, d, f, h, j) show the details of the fibre yarn, *i.e.,* twists in yarns and continuity of individual fibres.

temperatures from 25 °C to 170 °C at a frequency of 1 Hz. The deformation/dynamic strain was set to be constant at 0.2% under the cantilever mode.

3. Results and discussion

3.1. Morphology and microstructure of fabrics

Four types of fabrics were used in this work, including one silk fabric originally produced by a common silkworm species of *B. mori* and three hybrid fabrics of *B. mori* silk and flax fibre. As introduced, hybrid fabrics had three hybrid ratios of flax:silk, namely 21:79, 30:70 and 42:58 with increasing flax fraction. The woven structure of the fabrics is shown in the SEM micrographs in Fig. 2. These fabrics consisted of a normal plain-woven structure despite varied strand densities along two directions, and are similar to that used in previous studies [12,17,18]. *B. mori* silk fabric in Fig. 2(a,b) was tightly woven with little porosity between the fibres and between the fibre bundles. The neat and tightly woven structure of silk was proved to increase the fibre volume fraction in the composite up to 70 vol% [17]. Compared to pure silk fabrics, the three silk-flax hybrid fabrics in Fig. 2(e-j) were woven less tightly. Due to the high stiffness, non-continuity and poor elasticity, flax fibres in fabrics are often difficult to weave [38], and therefore are woven and twisted in relatively thick yarns, compared to continuous fibres. Flax fibres displayed a branched microstructure [5], which is shown in Fig. 2(c,d). In the hybrid fabrics of this work, by unravelling the hybrid fabrics we found that the flax fibres were woven into thicker yarns of 300–400 μm whereas the silk fibres were in thinner and more twisted yarns of ~300 μm in Fig. 2(f) and ~100 μm in Fig. 2(h–j). It was noted that the woven structure of the silk-flax hybrid fabric in Fig. 2(e, f) was distinctly different with 42% flax fraction; this woven structure was particularly effective in enhancing the mechanical properties of the composite, as discussed later. For the fabrication of hybrid fabric composites, a preferred direction along the thicker yarns of flax fibres

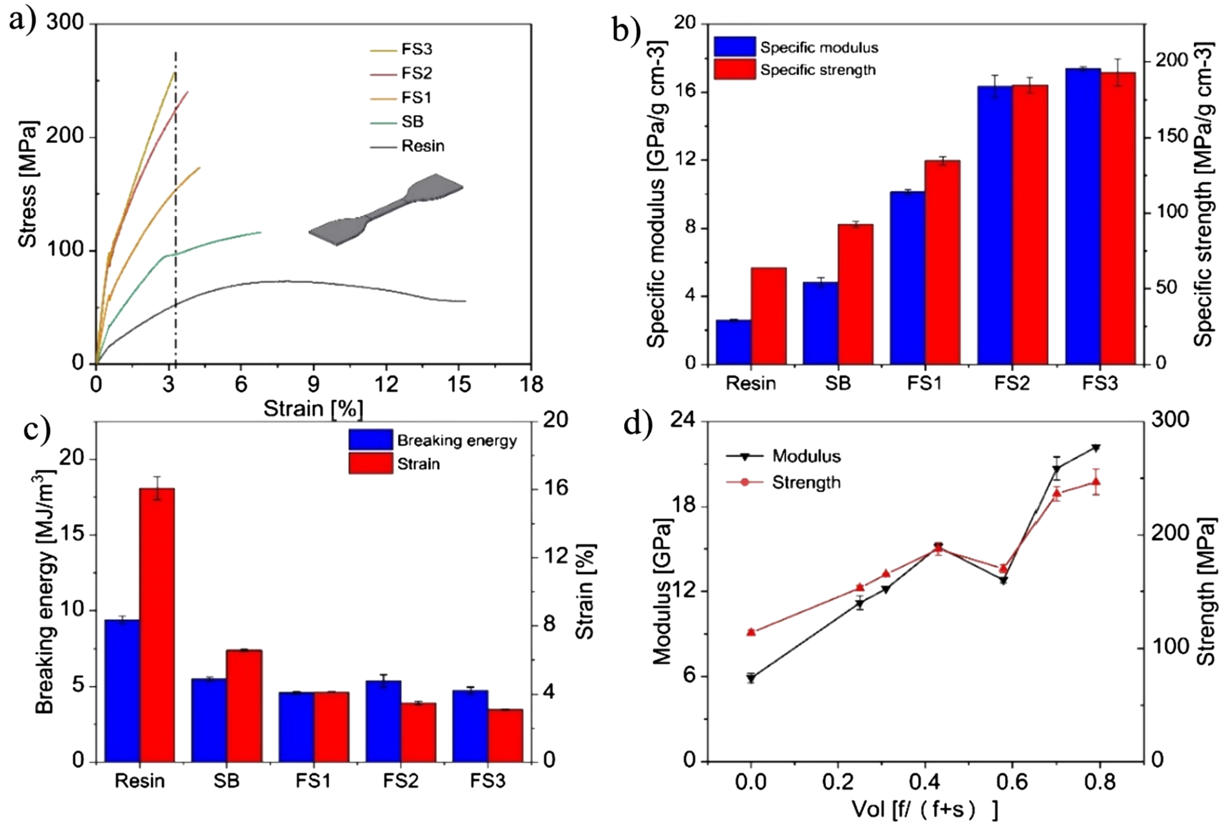

Fig. 3. Tensile mechanical properties of pristine epoxy resin, pure silk composites (*B. mori* silk fibre reinforced composites, SB) and intra-hybrid composites (FS1, FS2, FS3 with increasing flax fibre content). (a) Typical engineering tensile stress-strain curves. The inset shows the tensile specimen geometry. (b) Specific tensile modulus and specific tensile strength derived from stress-strain curves. (c) Breaking energy, calculated as the area under the stress-strain curves, and the strain at break. (d) Trendlines of the tensile modulus and strength evolving with the flax fibre fraction of the overall fibre reinforcement, expressed as $V_{[f/f+s]}$.

was noted as the longitudinal direction; this was also selected as the long-axis of the tensile and flexural test specimens to realize a maximum stiffening and strengthening effect of the flax fibres.

3.2. Mechanical properties of silk-flax hybrid fibre composites

3.2.1. Tensile mechanical properties

The geometry of tensile test specimens is shown in Fig. 3(a) and (b). The tensile stress-strain curves of pristine epoxy resin and various types of composites are shown in Fig. 3(c). For each material, at least three specimens were tested. The tensile mechanical properties, derived from the stress-strain curves, including Young's modulus, ultimate tensile strength, strain at break and breaking energy, are provided in linked data Table S1. Compared to the pristine epoxy resin, all the fibre reinforced composites in Fig. 3(d) displayed a higher tensile strength and modulus. The pristine (unreinforced) resin had an effective tensile elongation up to 8%, which can be considered as a high ductility. As the flax fraction increased from 21% to 42% from FS1 to FS3 of intraply laminates, the initial elastic modulus increased from 12.8 GPa to 22.2 GPa, and the tensile strength increased from 170 MPa to 247 MPa. However, the tensile elongation was seen to be lowered with increasing flax content.

Further using intercalated configurations of hybrid fabrics and silk fabrics, the flax fibre fraction in the composites was varied from 0 vol% to 80 vol%. Of note here is that stacking sequence was not found to be a significant influence on the tensile mechanical properties [7,11]. Fig. 3(f) summarizes the effect of flax fibre content on the properties, where it is evident that tensile modulus and strength show a linear increase as the flax fibre fraction increases. The exception is the FS1 hybrid composites with ~60% relative volume content of flax fibres, which display lower than expected stiffness and strength values, possibly due to their different fabric textile structure (Fig. 2(e)). It is also found that the breaking strains of the two super-hybrid configurations (SHS and HSH) with less flax were inferior to that of the intra-hybrid structure of FS2 with more flax. This agrees with the literature that flax fibres can induce catastrophic brittle fracture, which can lead to cracks along the flax-matrix interfaces and sequential failure of the other fibres [7,25]. However, when silk and flax fibres were intra-plied, e.g., in FS2, the silk fibres may act to prevent unstable cracking that originated in the flax fibres.

The microstructure of the fracture surfaces from tensile tests are shown in Fig. 4. The presence of residual epoxy debris on fibre surfaces indicate good fibre-resin adhesion [7]. All the FS laminates were found to show residual epoxy debris on the pull-out fibres. The detailed damage modes are also evident in this figure for each composite, including fibre and fibre yarn pull-out, matrix cracking and fibre-matrix interface damage. The SB composites showed smoother fracture surfaces than the FS hybrid composites (Fig. 4a). Fibre yarn pull-out is also indicated in the figure, which appeared more severe in the hybrid composites (Fig. 4(b–d)) compared to silk composites, suggesting better interfacial bonding of silk fibres with the resin compared to flax fibres. To summarize this section, a clear trend of increasing tensile modulus and strength was observed with increased flax content. The FS2 composite also displayed the highest tensile breaking energy among all the hybrid fibre composites, similar to that of the SB material.

3.2.2. Flexural mechanical properties

Silk-epoxy composites have been reported to possess superior flexural mechanical properties [16,18]. The flexural properties of pure silk composites, as compared to the intraply hybrid composites and the

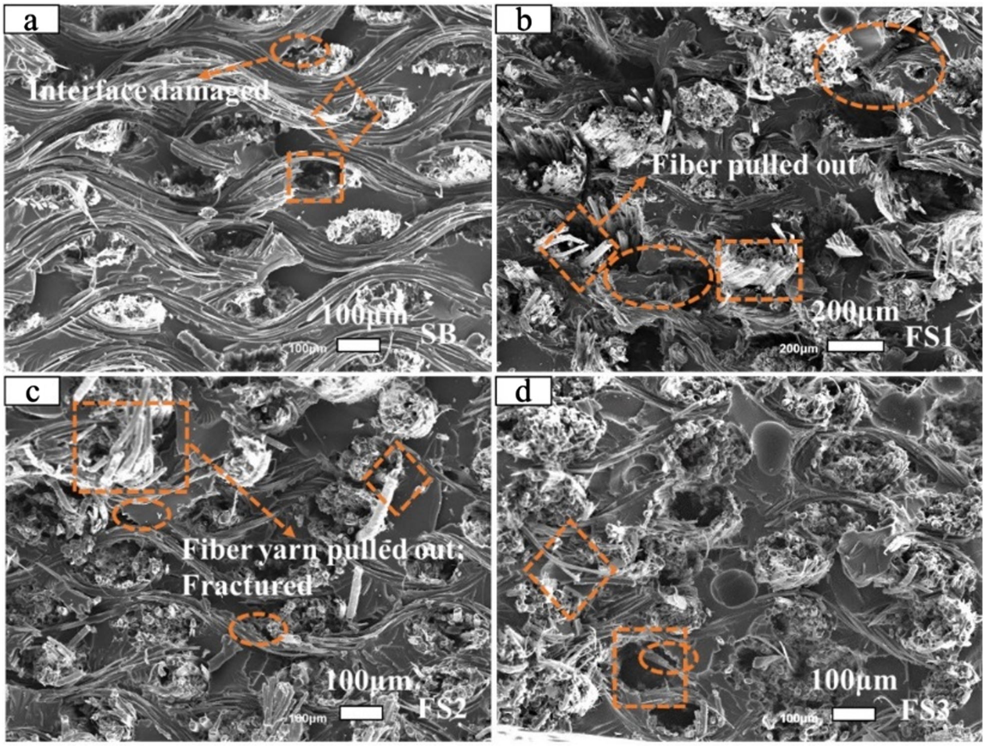

Fig. 4. Scanning electron microscope (SEM) images of tensile fracture morphologies including interfacial damage, fibre or fibre yarn pull-out and fracture of specimens from (a) SB composites and intraply hybrid composites (b) FS1, (c) FS2, (d) FS3.

pristine resin are presented in Fig. 5 and Table S1. For the three intraply hybrid composites, the flexural modulus and strength, akin to the tensile results, were improved by introducing flax fibres. In particular, the specific flexural modulus of the FS3 material was 320% higher than that of the SB composites. However, the flexural breaking strain for the intraply hybrids was lower; this differs from the tensile results due to the effect of the configuration of the laminates. It is generally accepted that plying laminates with relatively low modulus and high flexural failure strain, especially on the flexural surfaces, can significantly improve the flexural strength of hybrid composites [16,39]. However, the HSH super-hybrid composite (plying hybrid fabrics on the outside and pure silk in the middle) showed a high flexural strength owing to the stiffer flax on the out-layers of hybrid fabrics, and high flexural failure strain contributed by silk (Fig. 4(d)). Moreover, the FS3 composites that contained mainly high modulus flax and “complementary” low modulus silk fibres displayed in the highest flexural strength of 300 MPa, which is comparable to that in nonwoven plain glass fibres reinforced composites. This highlights the potential of natural fibres in enhancing the flexural properties of epoxy-resin reinforced composites.

The macroscopic flexural deformation and fracture mode of the composites, shown in the inset in Fig. 5(a), can be seen to markedly change with the hybrid ratios. Flexural failure modes include compressive, tensile and shear failures in the matrix, fibres and the interfaces [40]. In the present study, the span-to-thickness ratio (L/t) of ∼15 (32 mm/2.15 mm) suggests the main failure mode should be axial compressive damage under the loading roller [41]. However, cracks that originated at the far side under the loading roller could be associated with the tensile failure, as shown in Fig. 6. Silk SB composites displayed greater bending deformation and ductile failure features, such as irregular translaminar crack path and fibre-bridging (Fig. 6(a-2, 3)), as reported previously [7,11]. Silk fibres could blunt the crack front and deviate the crack path [30]. More silk micro-fibrils were also seen to contribute to the flexural breaking energy. The silk-flax intraply hybrid composites displayed less ductile failures, as shown in Fig. 6(b, c). In contrast, the FS3 composite displayed only semi-ductile fibre fractures with the presence of ductile silk fibres and brittle flax fibres in the same region in Fig. 6(c-3).

3.3. Interfacial properties of composites

The interfacial properties and the compatibility behaviour between fibre and resin are often evaluated by the inter-laminar shear test [42]. The inter-laminar shear strength (ILSS) results are shown in Table S1. The failure modes were a mix of shear and tensile fractures for all the composite specimens tested here. Therefore, the ILSSs here are not strictly comparable to the values from shear fracture-only tests. The ILSS of pure SB composites was the lowest at 26.9 MPa, and for the FS hybrid laminates, the ILSS increased from 31.2 MPa for FS1 to 36.0 MPa for FS3 as the fraction of flax fibre increased. Previous works [16,17] reported greater interfacial adhesion in silk-epoxy resin composites than flax-epoxy resin composites. It is suggested that the enhanced ILSS could be attributed mainly to the z-directional stiffness/modulus of the flax fibre. The same mechanism was revealed in another hybridization work of flax and glass fibres [11]. Notably, the ILSS of the intraply hybridization composites FS3 and the super-hybrid configuration with flax in the out-layers appeared higher, in which the z-direction stiffness of flax affects more effectively. We therefore reasoned that introducing flax fibres into these materials enhanced the interfacial shear performance of the composite mainly through a mechanism of enhancing the z-direction stiffness. Importantly, the ILSSs of silk-flax hybrid fibre composites in this work were comparable to that of glass fibre reinforced composites. In addition, compared with the lay-up process for fabricating silk-epoxy resin composites [17], VARTM may also contribute to improved interfacial adhesion through the flow infiltration of the epoxy resin, in agreement with the earlier reports on glass fibre reinforced composites [43,44].

The interfacial properties of the composites were also investigated using dynamic mechanical thermal analysis or DMTA, which is widely

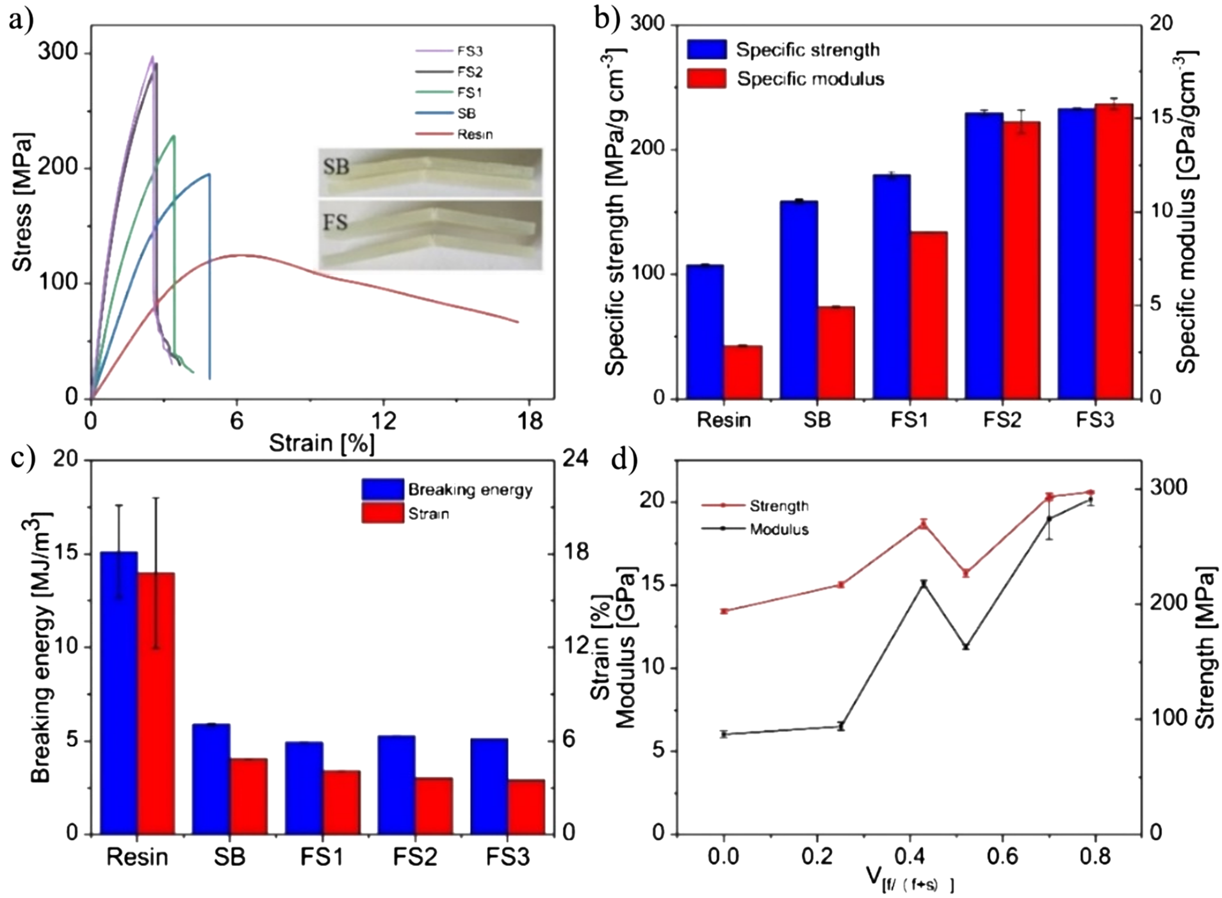

Fig. 5. Flexural properties of epoxy resin, the intraply hybrids and pure silk composites with ~50 vol% fibre reinforcement. (a) Typical flexural stress-strain curves. (b) Specific flexural modulus and specific flexural strength values. (c) Breaking energy and strain at break. (d) Flexural modulus and strength evolving with flax fibre fraction in the fibre reinforcement, expressed as $V_{[f/f+s]}$. Macroscopic fracture morphologies after flexural damages for the SB and FS composites are shown in inset of (a).

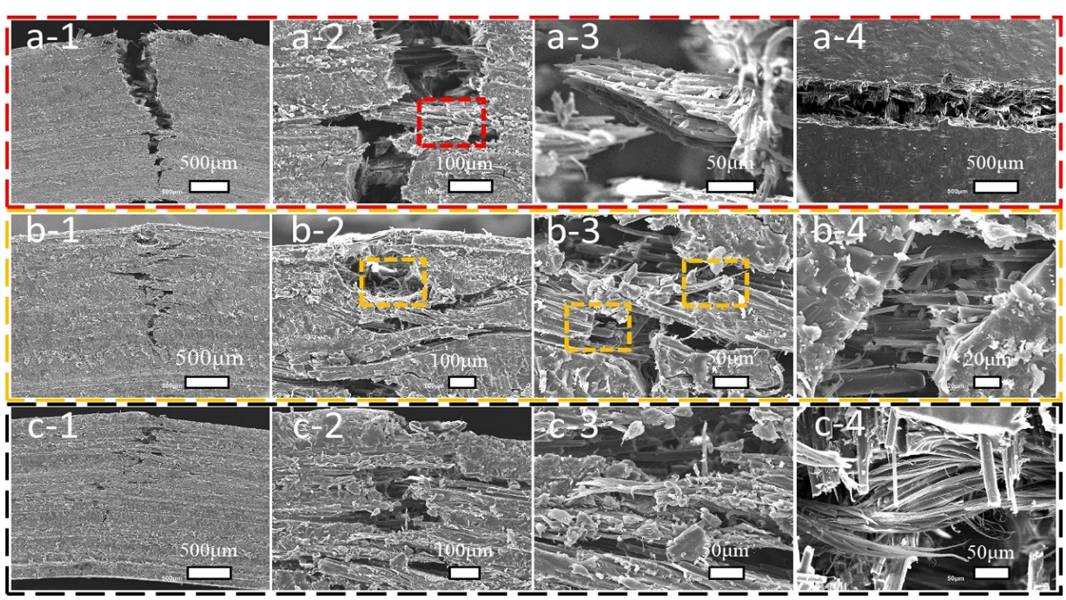

Fig. 6. Scanning electron microscopy (SEM) images of the flexural fracture microstructure of composite specimens in two directions, (a) SB, (a-1), (a-2) and (a-3) are side-views; and (a-4) is top-view. Fibre-bridging and resin debris can be observed in the square of red dashed lines (a-2). (b) Intraply composite FS1, (b-1), (b-2) and (b-3) are side-views; and (b-4) is top-view. Silk fibrillation is highlighted in the square in (b-2); flax's brittle fracture and silk's ductile fracture are also highlighted in the square in (b-3). (c) Intraply composite FS3, (c-1), (c-2) and (c-3) are side-views; (c-4) is top-view.

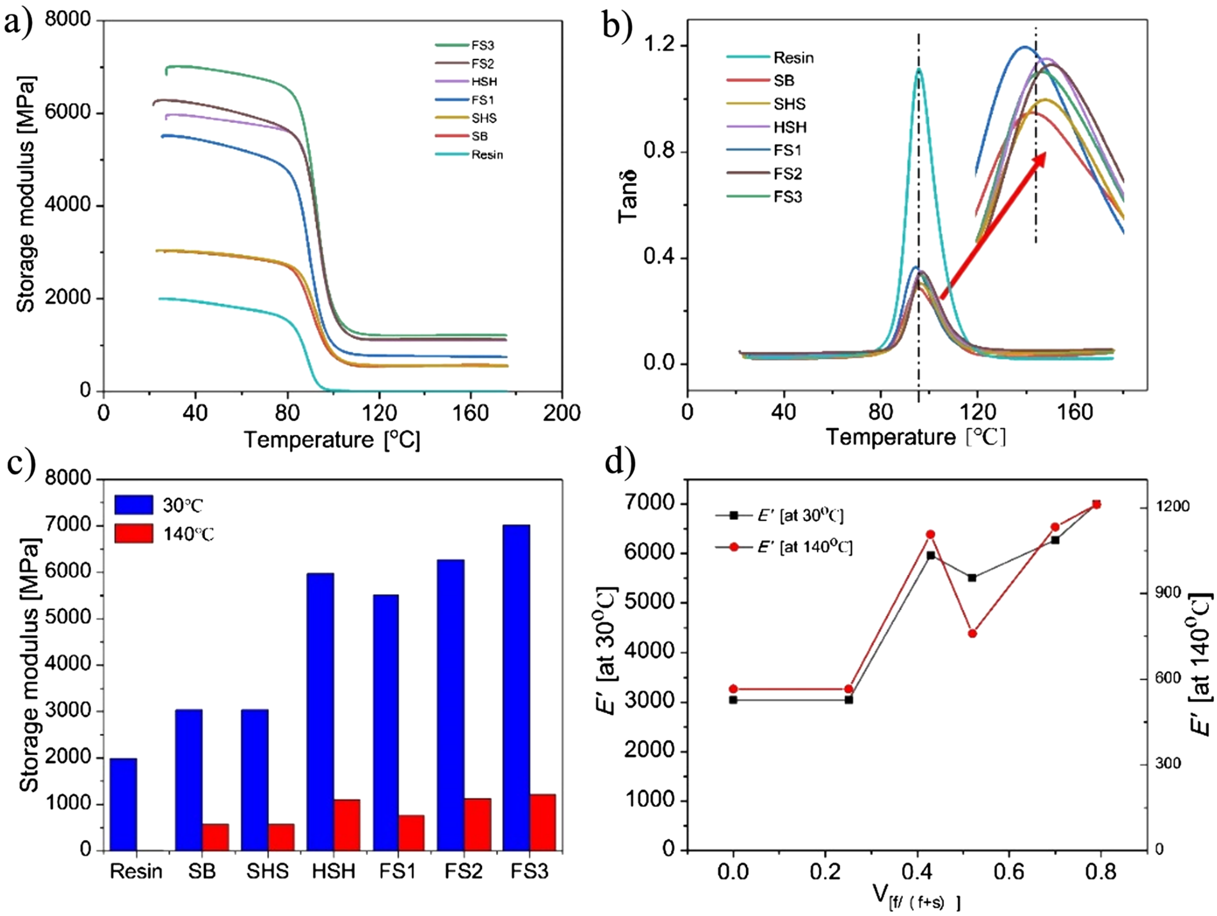

Fig. 7. Dynamic mechanical thermal analysis of epoxy resin, pure silk composite, intraply hybrid composites and super hybrid composites (HSH, SHS) from 25 °C to 170 °C: (a) storage modulus (E') as a function of temperature; (b) damping factor tanδ as a function of temperature; (c) storage modulus E' of epoxy resin and composites at 30 °C and at 140 °C corresponding to before and after the glass transition of epoxy resin; (d) storage modulus E' at 30 °C and 140 °C related with flax fibre fraction in the overall flax + silk fibre reinforcement, $V_{[f/(f+s)]}$.

used to characterize the structure, thermomechanical properties and viscoelastic responses of polymers and polymer composites [45,46]. Here, the glass-transition behaviours were analysed to better understand the interfacial bonding between the fibre reinforcements and the epoxy matrix [47,48]. Fig. 7 shows the dynamic mechanical storage modulus (E') and damping factor (tanδ) in Fig. 7(a) and (b), of the intra-hybrid composites, non-hybrid composites and super-hybrid composites through the glass transition. In Fig. 7(c) and (d), the storage modulus at 30 °C increased with increased flax content at $V_{[f/s+f]} > 0.2$. In particular, the FS3 material had the highest storage modulus of 7.0 GPa owing to its high stiffness and larger volume fraction of flax fibres. SHS and SB composites displayed a similar storage modulus because the 23% of flax fibres were placed in the middle in SHS and could not play the high-stiffness role under small dynamic deformations. Additionally, three hybrid composites, namely FS2, FS3 and HSH, maintained a storage modulus greater than 1 GPa above their glass-transition temperature T_g, which is important for many engineering applications.

The T_g of epoxy resin defined by peak tanδ in Fig. 7(b), was in a narrow region between 94 °C and 97.5 °C for all the silk and hybrid composites. The T_g of pristine epoxy resin was 95 °C and was slightly lower at 94 °C for SB and FS1 composites; by comparison, the T_g values for the remainder of the hybrid composites were shifted to a higher temperature (by ~2 °C). It is suggested that the height of the tanδ peak can indicate the “quality” of interfacial bonding. Strong interfacial bonding would restrict the molecular mobility of epoxy resin segments at T_g, thereby reducing the magnitude of the tanδ peak [47]. The FS1 composite showed the highest tanδ among the intra-hybridization composites, which suggests the poorest interfaces among FS1-3, consistent with its lowest ILSS.

Table 1
Charpy impact strength (kJ.m^{-2}) of silk and hybrid fibre composites.

Specimen	SB	SHS	HSH	FS1	FS2	FS3
Mean (kJ.m^{-2}) ± SD	23.08 ± 0.83	31.83 ± 3.42	31.62 ± 2.72	21.48 ± 2.51	28.83 ± 3.99	26.14 ± 1.98

3.4. Impact performance of composites

Silks are presumed to possess a high fracture strain capacity and thus the ability to both absorb and dissipate energy under impact events [13–15]. Here two impact test methods (Charpy impact and the falling weight impact) were used to evaluate the impact performance of the composites under dynamic conditions. The Charpy impact strengths, listed in Table 1, did not show a simple relationship with the flax content or laminate configuration. The silk composite SB and intraply hybrid FS1 had the lowest impact strength, whereas the super-hybrid fibre composites SHS and HSH had the highest impact strength, despite the fact that the latter composites had a lower flax content than the intraply composites FS1-3. Overall, introducing flax fibres to silk-epoxy

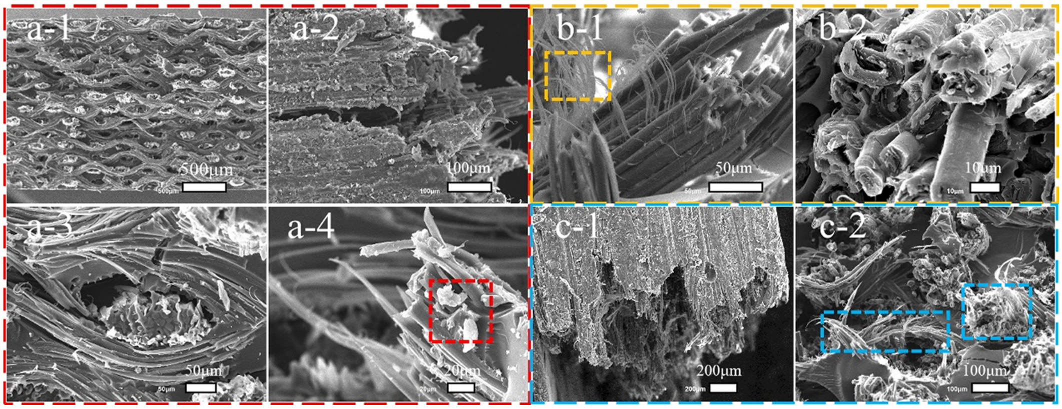

Fig. 8. Scanning electron microscopy (SEM) images showing the fracture microstructure after Charpy impact tests from two directions. (a) SB, (a-1, a-3) are top-views, (a-2, a-4) are side-views. Resin debris is highlighted in the square in (a-4). (b) FS1, (b-1, b-2) are top-views. Silk micro-fibrils are highlighted in the square in (b-1). (c) FS3, (c-1, c-2) are top-views. Silk fibrillation and flax fracture are highlighted in the squares in (c-2).

composites improved the Charpy impact strength, but to achieve an optimized impact strength the laminate configuration must also be considered.

The impact fracture morphology after Charpy impacts is shown in Fig. 8 from two directions representative of the impact direction for the SB, FS1 and FS3 composites. The energy absorption mechanisms for silk fibres under impact also include elastic and plastic deformation as well as fibrillation [49]. For the SB composites, fibre/yarn pull-out in Fig. 8(a − 1), matrix cracking in Fig. 8(a − 2), tightly packed silk yarn in Fig. 8(a − 3) and fibrillation of silk fibre in Fig. 8(a − 4) are seen. The considerable residual epoxy debris on the silk fibre surfaces indicates good adhesion between the fibre and epoxy resin under impact. For the intraply hybrid composites FS1 and FS3 (Fig. 8(b,c)), similar to the tensile fracture microstructure, the distinct fracture morphologies of the flax and silk fibres are seen. Nevertheless, the high-modulus flax fibres in hybrid composites (FS1-3), despite their brittle nature, still served to improve the Charpy impact performance of the silk-epoxy resin composites.

Falling weight impact tests were performed on pure silk composites SB, and three intraply hybrid composites FS1, FS2 and FS3 using 3 J and 4 J impact energies E_0. The representative damage fragmentations from the SB and FS1 composites after the falling weight impact test are shown in Fig. 9. All the laminates (including FS2 and FS3 specimens not shown here) displayed typical cross-shaped cracks on the front and back. The SB composites showed a smaller perforation depth of cross-shaped cracks, which signifies that the silk fibres absorbed more energy to prevent penetration of the impactor. The FS1 composite was penetrated, or even perforated, by the impactor and suffered the most severe damage after 4 J impact loading. Its fracture morphology, shown in the SEM image in Fig. 9(f), reveals fibrillated fibres and the almost disappearing epoxy resin matrix.

The crack size and area in Table 2 for the various composites can quantitatively indicate the extent of the impact damage. 4 J impacts resulted in larger crack sizes for all the specimens, as compared to 3 J impacts, consistent with previous studies [50]. Compared to the hybrid composites, the SB composites had the smallest crack sizes (47 mm/18 mm for 3 J impacts and 50 mm/29 mm for 4 J impacts) and the smallest crack area (664 mm^2 for 3 J and 1138 mm^2 for 4 J impacts). This again strongly implies the superior impact resistance of silk fibres. Moreover, the crack axis ratio (long-axis direction/short axis direction) of silk composites tended to be greater than the hybrid composites, suggesting more “directionality” in the propagation of the damage [23,51]. For the intraply hybrid composites, the crack area for 4 J impacts was seen to decrease with increasing volume fraction of flax fibres from FS1 to FS3. We accordingly conclude that hybridization with flax fibres in silk-epoxy resin composites may be beneficial for reducing impact damage.

Fig. 9 also showed the detailed load-time and energy-time profiles under impact. From the load (force)–time curves, the energy absorption can be calculated using the relationships described in ref. [50], which are found in Appendix II. The maximum load F_{max} in the load-time curves indicates the end of crack initiation and the start of crack damage propagation in the impact processes. Under 3 J impacts, SB and FS3 had the highest F_{max}, whereas for 4 J impacts, SB had the highest F_{max} of ∼320 N. The load-bearing capability of the intraply hybrid composites was consistent with the trend in crack areas; increasing flax content resulted in enhanced load-bearing capability and smaller damage regions. In addition, the SB and FS1 composites also showed more steps in load-time curve, which can be related to the damage processes in the silk fibres such as fibrillation. Nevertheless, pure silk composites SB showed superior load-bearing capability to almost all the intraply hybrid composites at both impact energies, which needs further investigation.

The absorbed energy in Fig. 9(i, j) showed that although SB composites displayed higher F_{max} under 4 J impacts, the FS3 hybrid composites exhibited the highest energy absorption during the impact process. For the 3 J impacts, the FS3 composites had an almost identical impact energy (also E_m) to the SB composites; however, for the 4 J impacts, the FS3 material first reached the highest energy in ∼10 ms whereas the silk composites absorbed energy more gradually and reached ∼4 J in ∼20 ms. It may imply that the flax fibres can faster absorb impact energy, therefore providing for more efficient energy absorption than purely silk reinforced composites under impact.

4. Conclusions

In this study, flax fibres were introduced into silk fibre reinforced epoxy resin composites via intraply and interply hybridization methods and vacuum-assisted resin transfer moulding. A clear trend of increasing modulus and strength of the hybrid composites under both tensile and flexural loading was observed with progressively increasing flax fibre content while the overall fibre volume fraction was maintained at 50 vol%. The interface property analyses revealed that introducing flax fibres into silk-epoxy resin composites can significantly improve the interlaminar shear strengths of the composites via enhancing the z-direction stiffness. Most importantly, the Charpy impact testing and falling weight impact testing showed that introducing flax fibres can enhance the impact strength compared to pure silk fibre reinforced and may also increase the efficiency in impact energy absorption. This study can provide insights into the application of silk in structural composites and bio-composites for biomedical use.

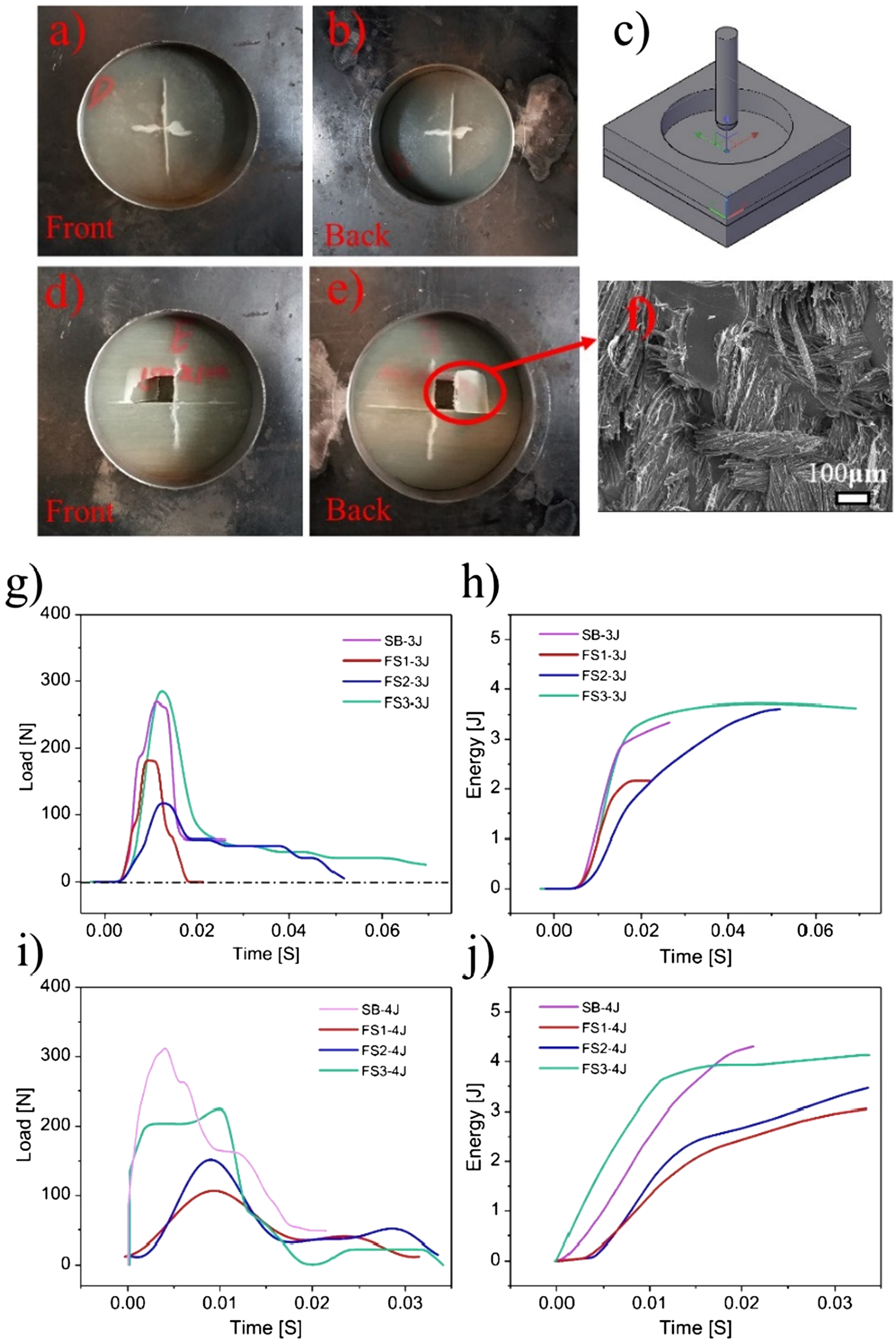

Fig. 9. Impact properties from falling weight impact tests (including damage fragmentation, load bearing capability and energy absorbing capability) of pure silk composites and intraply hybrid composites. (a, b) Macroscopic crack front and back surface of the SB composite under 4 J impacts. (c) Schematic diagram of the experimental set-up of falling weight test. (d, e) Macroscopic crack front and back surface of the FS1 material under 4 J impacts. (g, h) Comparison of load-time profiles under 3 J and 4 J impact, respectively. (i, j) Comparison of energy-time profiles for impact energies of 3 J and 4 J, respectively.

Table 2
Summary of crack length and crack area of composites after impact loading.

Specimen	SB	FS1	FS2	FS3	SB	FS1	FS2	FS3
Impact energy(J)	3	3	3	3	4	4	4	4
Crack length (mm/mm)	47/18	55/35	56/29	52/31	50/29	63/44	61/37	58/33
Crack area* (mm^2)	664	1511	1275	1265	1138	2176	1772	1502

* The crack area is the elliptical area surrounding the cross-shaped crack.

Acknowledgements

C.W., K.Y. and J.G. wish to thank the National Natural Science Foundation of China (no. 51503009) and Beihang University. Y.G. and J.X were supported by the National Natural Science Foundation of China, respectively under Grant nos. 51563013 and U1664250. R.O.R. acknowledges support from the U.S. Department of Energy, Office of Science, Office of Basic Energy Sciences, Materials Sciences and Engineering Division under Contract no. DE-AC02-05CH11231 to the Lawrence Berkeley National Laboratory (Mechanical Behavior of Materials program, KC 13).

Appendix I:. Chemical structures of the epoxy resins and hardeners

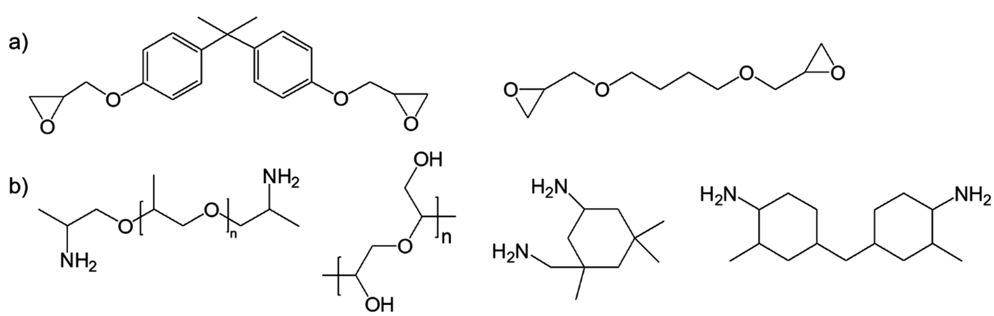

(a) Chemical structures of the epoxy system 1564 including a bisphenol epoxy and an aliphatic epoxy; (b) Chemical structure of the hardener system 3486.

Appendix II. : Equations for analyzing the falling weight experimental data [50]:

$$E_0 = mgh = \frac{mv_0^2}{2} \tag{1}$$

$$v(t) = v_0 + gt - \frac{1}{m}\int_0^t F(t)dt \tag{2}$$

$$\delta(t) = \delta_0 + v_0 t + gt^2/2 - \frac{1}{m}\iint_0^t F(t)dtdt \tag{3}$$

$$E(t) = \frac{m(v_0^2 - v(t)^2)}{2} + mg\delta \tag{4}$$

where E_0 is the initial impact energy, $E_{(t)}$ is the absorbed energy by the specimen, v andv_0 are, respectively, the velocity of the impactor at time t and $t = 0$, $F_{(t)}$ refers to the measured contact force at time t and δ is the displacement of the impactor.

Appendix B. Supplementary material

Supplementary data to this article can be found online at https://doi.org/10.1016/j.compositesa.2018.12.003.

References

[1] Yin S, et al. Introducing composite lattice core sandwich structure as an alternative proposal for engine hood. Compos Struct 2018;201:131–40.
[2] Sanjay M, et al. Characterization and properties of natural fiber polymer composites: a comprehensive review. J Cleaner Prod 2018;172:566–81.
[3] Lau K-T, et al. Properties of natural fibre composites for structural engineering applications. Compos B Eng 2018;136:222–33.
[4] Safri SNA, et al. Impact behaviour of hybrid composites for structural applications: a review. Eng Compos Part B 2017.
[5] Li Y, Xie L, Ma H. Permeability and mechanical properties of plant fiber reinforced hybrid composites. Mater Des 2015;86:313–20.
[6] Li Y, et al. Improved mechanical properties of carbon nanotubes-coated flax fiber reinforced composites. J Mater Sci 2015;50(3):1117–28.
[7] Kureemun U, et al. Effects of hybridization and hybrid fibre dispersion on the mechanical properties of woven flax-carbon epoxy at low carbon fibre volume fractions. Compos B Eng 2018;134:28–38.
[8] Saidane EH, et al. Damage mechanisms assessment of hybrid flax-glass fibre composites using acoustic emission. Compos Struct 2017;174:1–11.
[9] Sanjay M, Arpitha G, Yogesha B. Study on mechanical properties of natural-glass fibre reinforced polymer hybrid composites: a review. Mater Today: Proc 2015;2(4–5):2959–67.
[10] Petrucci R, et al. Mechanical characterisation of hybrid composite laminates based on basalt fibres in combination with flax, hemp and glass fibres manufactured by vacuum infusion. Mater Des 2013;49:728–35.
[11] Zhang Y, et al. Tensile and interfacial properties of unidirectional flax/glass fiber

reinforced hybrid composites. Compos Sci Technol 2013;88:172–7.
[12] Shah DU, Porter D, Vollrath F. Opportunities for silk textiles in reinforced biocomposites: Studying through-thickness compaction behaviour. Compos A Appl Sci Manuf 2014;62:1–10.
[13] Guan J, Porter D, Vollrath F. Silks cope with stress by tuning their mechanical properties under load. Polymer 2012;53(13):2717–26.
[14] Živković I, et al. Influence of moisture absorption on the impact properties of flax, basalt and hybrid flax/basalt fiber reinforced green composites. Compos B Eng 2017;111:148–64.
[15] Fragassa C, Pavlovic A, Santulli C. Mechanical and impact characterisation of flax and basalt fibre vinylester composites and their hybrids. Compos B Eng 2018;137:247–59.
[16] Shah DU, Porter D, Vollrath F. Can silk become an effective reinforcing fibre? A property comparison with flax and glass reinforced composites. Compos Sci Technol 2014;101:173–83.
[17] Yang K, et al. High volume-fraction silk fabric reinforcements can improve the key mechanical properties of epoxy resin composites. Mater Des 2016;108:470–8.
[18] Yang K, et al. Enhancing the mechanical toughness of epoxy-resin composites using natural silk reinforcements. Sci Rep 2017;7(1):11939.
[19] Guo C, et al. Structural comparison of various silkworm silks: an insight into the structure-property relationship. Biomacromolecules 2018;19(3):906–17.
[20] Senthilkumar K, et al. Mechanical properties evaluation of sisal fibre reinforced polymer composites: a review. Constr Build Mater 2018;174:713–29.
[21] Dhakal HN, et al. Effect of basalt fibre hybridisation on post-impact mechanical behaviour of hemp fibre reinforced composites. Compos A Appl Sci Manuf 2015;75:54–67.
[22] Hung P-Y, et al. Impact response of hybrid carbon/glass fibre reinforced polymer composites designed for engineering applications. Compos B Eng 2018;133:86–90.
[23] Sarasini F, et al. Drop-weight impact behaviour of woven hybrid basalt–carbon/epoxy composites. Compos B Eng 2014;59:204–20.
[24] Swolfs Y, et al. The importance of translaminar fracture toughness for the penetration impact behaviour of woven carbon/glass hybrid composites. Compos A Appl Sci Manuf 2017;103:1–8.
[25] Shahzad A. Impact and fatigue properties of hemp–glass fiber hybrid biocomposites. J Reinf Plast Compos 2011;30(16):1389–98.
[26] Kumar CS, et al. Effect of temperature and hybridisation on the low velocity impact behavior of hemp-basalt/epoxy composites. Compos Struct 2015;125:407–16.
[27] Ude A, Ariffin A, Azhari C. An experimental investigation on the response of woven natural silk fiber/epoxy sandwich composite panels under low velocity impact. Fibers Polym 2013;14(1):127–32.
[28] Noorunnisa Khanam P, et al. Tensile, flexural and compressive properties of sisal/silk hybrid composites. J Reinf Plast Compos 2007;26(10):1065–70.
[29] Rajkumar G, Srinivasan J, Suvitha L. Development of novel silk/wool hybrid fibre polypropylene composites. Iran Polym J 2013;22(4):277–84.
[30] Zhao D, et al. Flexural and hydrothermal aging behavior of silk fabric/glass mat reinforced hybrid composites. Fibers Polym 2016;17(12):2131–42.
[31] Ho M-P, Lau K-T. Design of an impact resistant glass fibre/epoxy composites using short silk fibres. Mater Des 2012;35:664–9.
[32] Yang Y, et al. Mechanical and optical properties of silk fabric/glass fiber mat composites: an artistic application of composites. Text Res J 2017. 0040517517690621.
[33] Smitthipong W, et al. Interesting green elastomeric composites: Silk textile reinforced natural rubber. Polym Test 2016;55:17–24.
[34] Chen Q, et al. Mechanical properties in glass fiber PVC-foam sandwich structures from different chopped fiber interfacial reinforcement through vacuum-assisted resin transfer molding (VARTM) processing. Compos Sci Technol 2017;144:202–7.
[35] Kelkar AD, Tate JS, Chaphalkar P. Performance evaluation of VARTM manufactured textile composites for the aerospace and defense applications. Mater Sci Eng, B 2006;132(1–2):126–8.
[36] Dehkordi MT, et al. The influence of hybridization on impact damage behavior and residual compression strength of intraply basalt/nylon hybrid composites. Mater Des 2013;43:283–90.
[37] Bensadoun F, et al. Low velocity impact properties of flax composites. Compos Struct 2017;176:933–44.
[38] Shah DU, Schubel PJ, Clifford MJ. Can flax replace E-glass in structural composites? A small wind turbine blade case study. Compos B Eng 2013;52:172–81.
[39] Kalantari M, Dong C, Davies IJ. Numerical investigation of the hybridisation mechanism in fibre reinforced hybrid composites subjected to flexural load. Compos B Eng 2016;102:100–11.
[40] Caminero M, Rodríguez G, Muñoz V. Effect of stacking sequence on Charpy impact and flexural damage behavior of composite laminates. Compos Struct 2016;136:345–57.
[41] Carbajal N, Mujika F. Determination of compressive strength of unidirectional composites by three-point bending tests. Polym Test 2009;28(2):150–6.
[42] Wang Z, Xian G, Zhao X-L. Effects of hydrothermal aging on carbon fibre/epoxy composites with different interfacial bonding strength. Constr Build Mater 2018;161:634–48.
[43] Naik N, Sirisha M, Inani A. Permeability characterization of polymer matrix composites by RTM/VARTM. Prog Aerosp Sci 2014;65:22–40.
[44] Belingardi G, Cavatorta MP, Paolino DS. Repeated impact response of hand lay-up and vacuum infusion thick glass reinforced laminates. Int J Impact Eng 2008;35(7):609–19.
[45] Wang Y, et al. Understanding the variability of properties in Antheraea pernyi silk fibres. Soft Matter 2014;10(33):6321–31.
[46] Duc F, et al. Damping of thermoset and thermoplastic flax fibre composites. Compos A Appl Sci Manuf 2014;64:115–23.
[47] Gu H. Dynamic mechanical analysis of the seawater treated glass/polyester composites. Mater Des 2009;30(7):2774–7.
[48] Saba N, et al. A review on dynamic mechanical properties of natural fibre reinforced polymer composites. Constr Build Mater 2016;106:149–59.
[49] Reghunadhan A, et al. Toughness augmentation by fibrillation and yielding in nanostructured blends with recycled polyurethane as a modifier. Appl Surf Sci 2018;442:403–11.
[50] Ude A, Ariffin A, Azhari C. Impact damage characteristics in reinforced woven natural silk/epoxy composite face-sheet and sandwich foam, coremat and honeycomb materials. Int J Impact Eng 2013;58:31–8.
[51] Liang S, Guillaumat L, Gning P-B. Impact behaviour of flax/epoxy composite plates. Int J Impact Eng 2015;80:56–64.